
Article

Not peer-reviewed version

Retrospective Evaluation of Subpleural Consolidations Using Lung Ultrasound in 634 Dogs and 347 Cats

[Katarzyna Kraszewska](#) ^{*}, [Michał Gajewski](#), [Søren Boysen](#), [Natalia Buda](#)

Posted Date: 4 February 2025

doi: [10.20944/preprints202405.0145.v2](https://doi.org/10.20944/preprints202405.0145.v2)

Keywords: consolidation; color Doppler; vascularity; bronchogram



Preprints.org is a free multidisciplinary platform providing preprint service that is dedicated to making early versions of research outputs permanently available and citable. Preprints posted at Preprints.org appear in Web of Science, Crossref, Google Scholar, Scilit, Europe PMC.

Copyright: This open access article is published under a Creative Commons CC BY 4.0 license, which permit the free download, distribution, and reuse, provided that the author and preprint are cited in any reuse.

Disclaimer/Publisher's Note: The statements, opinions, and data contained in all publications are solely those of the individual author(s) and contributor(s) and not of MDPI and/or the editor(s). MDPI and/or the editor(s) disclaim responsibility for any injury to people or property resulting from any ideas, methods, instructions, or products referred to in the content.

Article

Retrospective Evaluation of Subpleural Consolidations Using Lung Ultrasound in 634 Dogs and 347 Cats

Katarzyna Kraszewska ^{1,*}, Michał Gajewski ¹, Søren Boysen and Buda Natalia ²

¹ Vetcardia Veterinary Clinic Kijowska 11, 03-743 Warsaw, Poland

² Simulation Laboratory of Endoscopic and Minimally Invasive Techniques, Medical University of Gdańsk, Poland

* Correspondence: Katarzyna Kraszewska Vetcardia Veterinary Clinic Kijowska 11, 03-743 Warsaw, Poland; pavc.info@gmail.com

Abstract: *Background:* Human literature describes vascular patterns in various types of lung consolidations; however, these changes have not been analyzed in dogs and cats. This retrospective analysis of medical records aimed to describe vascular patterns observed in the airless subpleural lung tissue of dogs and cats and to compare these patterns to various lung consolidations and clinical diagnoses according to parenchymal and vascular criteria described in the human literature. *Animals:* 347 cats and 634 dogs. *Methods:* This was a retrospective study encompassing medical records obtained between 2018 and 2023. Lung ultrasound was performed in dogs and cats and cases with different sonographically identified airless subpleural lung tissue were selected. Lung consolidations were classified as shred, nodule, wedge sign, mass, and tissue sign. Further classification was based on the parenchymal criteria, the presence or absence of bronchograms and the vascular patterns identified within these regions. Bronchograms were classified as air bronchograms (dynamic and/or static), fluid bronchograms, mixed fluid and air bronchograms, and/or absence of bronchograms. Vascular patterns were classified as tree-like, residual, chaotic, “vascular sign,” and whether they were continuous with and extended from the chest wall or not. *Conclusions and Clinical Importance:* It is possible to identify and characterize airless subpleural lung tissue in cats and dogs based on the parenchymal and vascular characteristics.

Keywords: consolidation; color Doppler; vascularity; bronchogram

Introduction

The exponential use of ultrasound, the availability of devices, and the popularization of point-of-care ultrasonography (POCUS) make lung ultrasound (LUS) examination a rapidly evolving diagnostic modality [1,2]. In veterinary medicine there is limited literature describing the utility of LUS in diagnosing parenchymal lung diseases associated with lung consolidations in small animal patients [3–7]. By contrast, LUS has been thoroughly studied in human medicine and is considered an essential tool for increasing diagnostic accuracy in dyspneic patients [8,9]. According to newly published human guidelines, the first diagnostic approach in patients with acute dyspnea should include thoracic ultrasound [10]. It allows differential diagnosis between potentially life-threatening conditions such as pulmonary edema and bronchopneumonia and can help assess the severity of lung injury [10–13]. This retrospective study analyzed airless subpleural lung tissue using B-mode and color Doppler, according to parenchymal and vascular criteria.

The primary objective was to analyze and describe subpleural consolidations and lung atelectasis in dogs and cats according to their shape and margins, along with parenchymal and vascular criteria. The secondary objective was to determine if sonographic assessment of vascular



criteria within airless subpleural lung tissue is feasible in dogs and cats and determine if vascular criteria differ between shred, tissue, nodule, wedge sign, and mass lesions.

Materials and Methods

Study Population

This retrospective study included cats and dogs that presented to the Vetcardia cardiorespiratory clinic in Warsaw between May 2018 and December 2023. The patient database was mined for all patients who had both echocardiographic and non-echocardiographic thoracic ultrasound performed. A total of 45148 patients were identified. All non-canine or feline patients and cases without subpleural consolidations in the description were excluded, leaving 2157 patients. Cases with incomplete records that did not include a final diagnosis or follow-up were also excluded, leaving 634 dogs and 347 cats.

Ultrasound Machine Settings and Probe Selection

All thoracic ultrasound examinations were performed using GE Vivid IQ machines; various phased-array probes (12MHz, 6MHz, or 3MHz) were utilized for echocardiography, while LUS was performed with a multifrequency linear probe (12L). Assessment of airless subpleural lung tissue was performed using the linear probe using both "lung" and "thyroid" presets. The "lung" preset has harmonics turned off, uses the lowest frequency setting (6MHz), has persistence set at zero, and a focal point positioned centrally within the consolidation [14–16]. The "thyroid" preset has harmonics and spatial compound imaging turned on, utilizes the high-frequency range of the probe, has a higher dynamic range, and has persistence set at 3; the preset was fine-tuned in each patient by positioning the focal point at the center of the consolidation. The "lung" preset creates a coarser image with better visibility of vertical artifacts, while the thyroid preset allows more detailed visualization of the echogenicity of airless lung tissue. The assessment of vascularity using Color or Power Doppler (CD/PD) mode was performed with both presets. The Doppler window was focused over regions of consolidation to detect flow signals [17]. The blood flow in a vessel was seen as a persistent area of color signal with a tubular, curvilinear, or branching distribution in real-time; color signals that persisted in the same location during the respiratory cycle were considered to be blood flow signals and not due to interference [17]. The CD/PD mode was set to the higher frequency of the Doppler mode and low pulse repetition frequency, which corresponded to a Nyquist limit of 0.07 – 0.09 m/s.

LUS Examination Technique

Six veterinarians performed echocardiography and LUS. The echocardiography examination was performed referred to the literature as "best practice" based on ACVIM consensus plus problem-oriented echocardiography [18,19]. Three of them had >15 years of experience in echocardiography (including KK, MG), were trained in LUS by a human specialist (NB) and had over 5 years of experience in LUS; one had >5 years of experience in echocardiography, was trained in LUS by a human specialist (NB), and had >2 years of experience in LUS, and one had > 5 years' experience in echocardiography and > 2 years of experience in LUS. The animals were examined in either sternal or lateral recumbency, depending on the severity of dyspnea. A combination of alcohol and gel was used as the coupling agent. The fur was not clipped.

Lung ultrasound examination was performed with a sliding protocol involving the placement of the linear probe in three horizontal lines on each hemithorax, as previously described by Kraszewska et al (Figure 1A, 1B, 1C, 1E) [3].

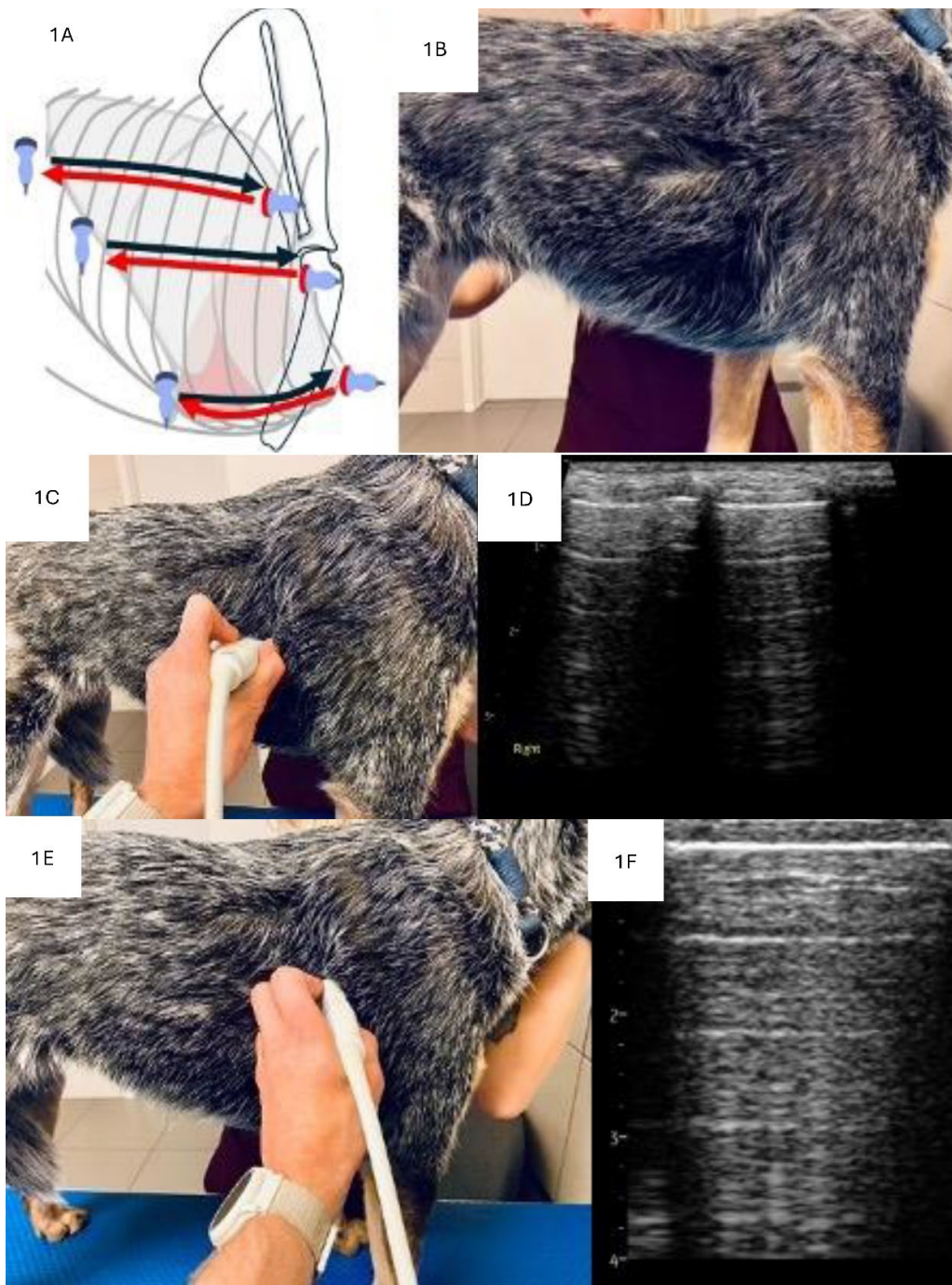


Figure 1. Lung ultrasound examination technique. 1A, Schematic representation of the location of the 3 scanning lines on a dog's thorax. Red and black arrows described the direction of the sliding of the transducer. 1B Photo of a dog with the fur parted and alcohol applied at the level of the middle scan line. 1C Position of the transducer perpendicular to the ribs (frontal plane) with corresponding sonogram (1D). 1E Position of the transducer parallel to the ribs (transverse plane) with corresponding sonogram (1F).

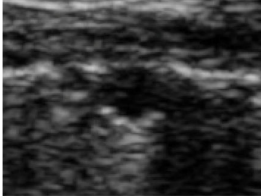
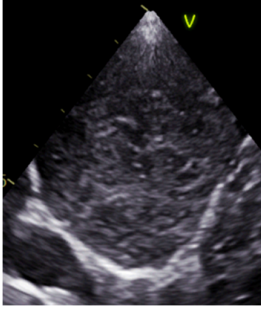
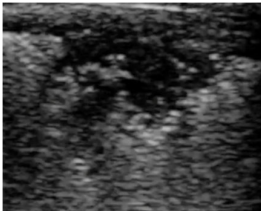
Analysis of Consolidations in 2D

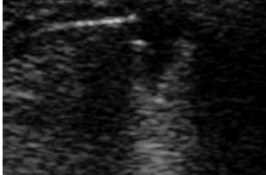
The airless subpleural lung tissue was assessed in 2D mode according to its shape, margins, and parenchymal criteria. Whenever airless subpleural lung tissue was described, its location on the left or right hemithorax was recorded, and for the statistical analysis, the lungs were divided into three zones: cranial, middle, and caudal (approximately 1/3 of the thoracic cavity length for each of the

zones). The size of the airless subpleural lung tissue didn't influence its classification; however, it was measured and reported in two dimensions: depth (the distance between the pleural line and the lower margin of the consolidation) and width (the diameter of the consolidation at the level of the pleural line) for monitoring purposes.

Terminology from previously published human and veterinary studies was used to describe the shape of airless lung tissue, which is a broad term encompassing all non-aerated subpleural regions of the lung. Airless lung tissue was initially classified as either atelectasis (i.e. the tissue [T] sign) or subpleural consolidations (i.e. airless lung tissue created by pathologic processes in the lung parenchyma). The latter was further divided into the shred (S) sign, the wedge (W) sign, and the nodule (N) sign; also, for the sake of this study, an additional category of a mass (M) was created [20–23]. The mass sign was differentiated from the nodule sign by the echogenicity of the airless lung tissue; the nodule sign was described as a round hypoechoic consolidation with smooth margins, while the mass sign was characterized as having a heterogeneous echogenicity and smooth margins. The characteristics of various types of airless subpleural lung tissue are presented in Table 1. In some patients, a combination of different consolidation types was observed during the examination within one area of a non-aerated lung. These were classified as complex lesions, i.e., tissue and mass (T/M), shred and nodule (S/N), and other combinations [24]. Complex lesions could exist together in the lung lobe and were often classified as a secondary change in the lung as a consequence of the primary pathology (i.e., a mass as one type of consolidation and a tissue sign peripheral to the mass as a secondary lesion due to associated resorption atelectasis).

Table 1. Characterization of different types of airless lung tissue.

Type of airless lung tissue	Morphology	Types of bronchogram	Echogenicity	Margins
Nodule		-No bronchogram	Hypoechoic	Smooth
Mass		-No bronchogram	Varied	Smooth
Shred		-Air dynamic -Air dynamic and static	Hypoechoic	Irregular

Tissue		-Air static -Fluid -Air static and fluid	Varied	Smooth
Wedge		-No bronchogram	Hypoechoic	Smooth

Furthermore, when present, the presence of air bronchograms were noted and subclassified within regions of airless subpleural lung tissue. In the human literature, three types of bronchograms exist: dynamic air bronchogram, static air bronchogram, and fluid bronchogram [8]. Dynamic air bronchograms are defined as hyperechoic structures visible in inspiration and disappearing on expiration; static air bronchograms represent the presence of air in the bronchial tree that is visible throughout both phases of respiration, and fluid bronchograms are formed due to the presence of fluid in the bronchial tree [8]. The consolidation was categorized as lacking a bronchogram when no visible hyperechoic (air) or hypoechoic (fluid) tree-like structure resembling a bronchial tree was visible within the consolidation. If more than one type of bronchogram was visible within a consolidation, these were described as complex findings for statistical analysis, e.g., dynamic and static air bronchogram, fluid bronchogram and the absence of bronchogram, and other combinations.

Analysis of Consolidations in Color/Power Doppler Mode

Regions of airless subpleural lung tissue were also classified according to the vascular criteria using the CD/PD mode. The presence or absence of blood flow in the non-aerated lung tissue and the spatial structure of the vascularization were assessed [25,26]. Five distinct vascular patterns were described within the airless lung tissue: anatomical tree-like vascularization, residual vascularization, chaotic vascularization, vascularization penetrating from the chest wall into the consolidation, and blood flow amputation, referred to as the "*vascular sign*." Tree-like vascularization is characterized by prominent, dilated blood vessels branching toward the lung's periphery, creating images that resemble a tree (Figure 2A, Movie 1). Residual vascularization is described as the presence of tree-like vessels but significantly less prominent and present only in some portions of the airless lung tissue (Figure 2B, Movie 2). Chaotic vascularization is created by tiny blood vessels coursing through the consolidation in various directions without any resemblance to the normal anatomy of the lung (Figure 2D). Penetrating vascularization is characterized by one or more vessels connecting the intercostal arteries with the consolidation (Figure 2C, Movie 3). The "*vascular sign*" (Figure 2E, Movie 4) is believed to result from vessel occlusion by embolic material [3,26,27]. Abrupt cessation of blood flow at the "tip" (i.e. the narrow, centrally located end) of the consolidation can be seen in CD/PD. In some cases, the blood flow profile was assessed using pulsed wave Doppler mode [28] to differentiate residual and chaotic vascularization [29]. Chaotic vascularization is characterized in human medicine as having a low velocity and low resistance flow profile in pulsed wave Doppler analysis [17,25,29,30].

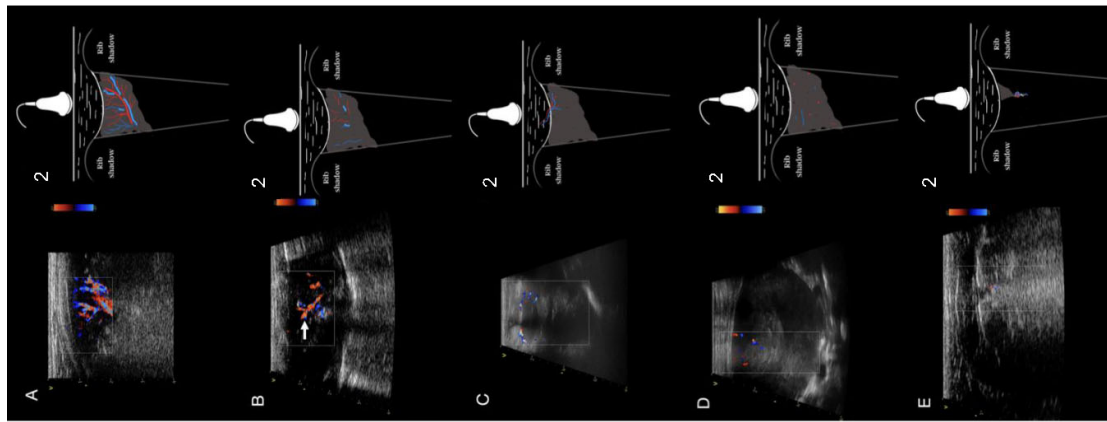


Figure 2. 2A-Linear probe, lung preset, longitudinal view. Still image, color Doppler imaging of the anatomical tree- like vascularization in a dog with pneumonia. Corresponding schematic diagram showing the tree-like vascularization within a region of consolidation- transverse view. 2B. Linear probe, lung preset, longitudinal view. Still image, color Doppler imaging of the residual vascularization (white arrow) within a region of consolidation. Corresponding schematic diagram showing a residual vascularization pattern within a region consolidation – transverse view. 2C. Linear probe, thyroid preset, longitudinal view. Still image, color Doppler imaging of a penetrating vascular pattern extending from the chest wall in a dog with a tumor. Corresponding schematic diagram showing a penetrating vascular pattern extending from the chest wall – transverse view. 2D. Linear probe, thyroid preset, longitudinal view. Still image, color Doppler imaging of a chaotic vascular pattern within a region of consolidation in a dog with a tumor. The diagram shows the chaotic vascularization in consolidation – transverse view. 2E. Linear probe, lung preset, longitudinal view. Still image, color Doppler imaging of the vascular sign in consolidation. Corresponding schematic diagram showing a vascular sign within a region of consolidation – transverse view.

Diagnosis

Depending on the presumptive diagnosis, various additional tests were performed, including echocardiography, thoracic radiographs (TXR), computed tomography (CT), bronchoscopy with bronchoalveolar lavage (BAL), fine needle aspiration (FNA), and cytology, histopathology, bacterial cultures, complete blood count and serum biochemistry, C-reactive protein level, D-dimers, and autopsy. The final diagnoses included pneumonia, interstitial lung disease (ILD), pulmonary neoplasia, metastatic disease, granuloma, abscess, acute respiratory distress syndrome (ARDS), pulmonary thromboembolism (PTE), congestive heart failure (CHF), and atelectasis. CHF was diagnosed based on an increased resting respiratory rate above 30/min, tachycardia and results of a full echocardiographic examination including: 2D, M-mode, Simpson method of disc, and diastolic function assessment. Metastatic and tumor diagnoses were confirmed by radiographs and/or CT, oncologist interpretation of FNA and/or histopathology examination, and subsequent response to treatment. A diagnosis of PTE was made based on D-dimer analysis, the presence of spontaneous echocontrast in the right atrium, and autopsy results in euthanized animals. Pneumonia was confirmed through CBC and/or CRP results, TXR at the referring clinic (TXR was repeated only in chronic symptoms or in cases unresponsive to treatment), BAL with bacteriology, and bronchoscopy, or a combination of the above. In a few cases a positive reaction to antibiotic treatment was considered supportive of pneumonia [6]. Granuloma was diagnosed with FNA or when consolidations resolved during treatment based on serial LUS examination [3]. Animals diagnosed with ARDS had severe bilateral diffuse changes with spared regions on LUS, hypoxia, and no evidence of left sided CHF based on echocardiography.

Statistical Analysis

Statistical analyses were performed using the IBM SPSS Statistics 29 package. Frequency analysis and basic descriptive statistics were performed. Chi-square tests of independence were used for comparisons with nominal variables and a Kruskal-Wallis test for quantitative variables. The level of significance was set at $\alpha = 0.05$. Standardized residuals with values lower than -1.96 and higher than 1.96 were considered statistically significant. Based on the values of standardized residuals, the range of P values was determined, where the value in the ranges $1,96 < \text{standardized residual} < 2,58$ stands for $P < 0,050$; $2,58 < \text{standardized residual} < 3,09$ equals $P < 0,010$, and $3,09 < \text{standardized residual}$ is $P < 0,001$.

Results

Characteristics of the Study Group

The study included 981 cases: 55% males, 45% females, 64.6% dogs and 35.4% cats. Age ranged from 1 month to 20.3 years ($M = 10.63$; $SD = 4.44$). Dog breeds varied but mixed-breed (28.2%) and Yorkshire Terriers (14.7%) were over-represented. Domestic Shorthair (DSH) (38.9%) and mixed-breed (26.5%) were the most common cat breed. Detailed percentage distributions of breeds are presented in Table 2.

Table 2. Percentage distribution of dog and cat breeds.

Species	Breed	<i>n</i>	%
Canine	Mix breed	179	28.20%
	Yorkshire Terrier	93	14.70%
	Cavalier King Charles Spaniel	35	5.50%
	West Highland White Terrier	29	4.60%
	Miniature Schnauzer	23	3.60%
	French Bulldog	21	3.30%
	Chihuahua	20	3.20%
	Shih Tzu	19	3.00%
	Dachshund	18	2.80%
	Jack Russell Terrier	17	2.70%
	Border Collie	15	2.40%
	Maltese	15	2.40%
	Beagle	11	1.70%
	German Shepard	11	1.70%
	Labrador Retriever	10	1.60%
Feline	Pug	10	1.60%
	Maltipoo	8	1.30%
	Miniature Pincher	8	1.30%
	Other breeds	92	14.5%
	DSH	135	38.90%
	Mix breed	92	26.50%
	Maine Coon	31	8.90%
	BSH	24	6.90%

Persian	20	5.80%
Syberian	14	4.00%
Oriental	5	1.40%
Ragdoll	5	1.40%
NFC	5	1.40%
Sphinx	5	1.40%
RBC	4	1.20%
Other breeds	9	2.10%

Abbreviations: BSH- British shorthair; DSH- domestic shorthair; n - number of observations; NFC – Norwegian forest cat; p - statistical significance; other breeds - breeds with six or fewer individuals; RBC - Russian blue cat.

Analysis of the Consolidations

The distribution and occurrence of consolidations are reported in Table 3. The most common simple consolidation was the shred sign (47.1%), while the least common was the wedge sign (2.6%); among complex consolidations, the combination of a shred and tissue sign (14.8%) were most often identified, with the combination of the nodule and wedge sign being the least commonly identified (0.1%).

Table 3. Percentage of individual types of airless lung tissue.

Consolidation type	<i>n</i>	%
Shred	460	47.10%
Shred/Tissue	145	14.80%
Mass	99	10.10%
Nodule	82	8.40%
Tissue	77	7.90%
Mass/Tissue	32	3.30%
Wedge	25	2.60%
Shred/Wedge	19	1.90%
Mass/Nodule	18	1.80%
Shred/Nodule	13	1.30%
Nodule/Tissue	4	0.30%
Tissue/Wedge	4	0.30%
Nodule/Wedge	2	0.10%
All	981	100.0%

Analysis of Bronchograms

The classification of bronchograms in airless lung tissue are presented in Table 4. There was a statistically significant difference between the type of bronchogram identified within different types of airless lung tissue. The observed effect was strong ($V_c > 0.50$). Dynamic bronchograms were reported more frequently with shred signs than other types of airless lung tissue ($P<0,001$). Within tissue signs, static and fluid bronchograms, and a combination of static and fluid bronchograms, were most often observed ($P<0,001$). Within mass, nodule, and wedge signs, the absence of bronchograms

was most commonly observed ($P<0.001$). For complex lesions, a mixed type of bronchogram was observed more often within the combined shred and tissue sign. In these consolidation types, dynamic and static, or dynamic, static, and fluid bronchograms were also observed. In the combined mass and nodule complex lesions, the absence of bronchograms was most often observed, while the static and the absence of bronchograms were most often reported within the combined shred and nodule complex lesions.

Table 4. Bronchograms identified within different types of airless lung tissue.

Bronchogram classification		Consolidation type										χ^2	<i>p</i>	Vc
		S	S/T	M	N	T	M/T	W	S/W	M/N	S/N			
Absent (n = 219)	<i>n</i>	3	1	89	76	0	11	17	4	15	3	2073.85	<0.001	0.57
	%	1.0%	0.7%	93.7%	97.4%	0.0%	34.4%	94.4%	30.8%	93.8%	27.3%			
Dynamic (n = 230)	<i>n</i>	229	1	0	0	0	0	0	0	0	0	2073.85	<0.001	0.57
	%	73.2%	0.7%	0.0%	0.0%	0.0%	0.0%	0.0%	0.0%	0.0%	0.0%			
Static (n = 42)	<i>n</i>	18	5	0	0	17	0	0	1	0	1	2073.85	<0.001	0.57
	%	5.8%	3.5%	0.0%	0.0%	23.9%	0.0%	0.0%	7.7%	0.0%	9.1%			
Fluid (n = 16)	<i>n</i>	1	0	0	0	13	2	0	0	0	0	2073.85	<0.001	0.57
	%	0.3%	0.0%	0.0%	0.0%	18.3%	6.3%	0.0%	0.0%	0.0%	0.0%			
Dynamic and static (n = 137)	<i>n</i>	59	73	1	0	1	1	0	0	0	2	2073.85	<0.001	0.57
	%	18.8%	50.7%	1.1%	0.0%	1.4%	3.1%	0.0%	0.0%	0.0%	18.2%			
Static and fluid (n = 52)	<i>n</i>	3	11	0	0	38	0	0	0	0	0	2073.85	<0.001	0.57
	%	1.0%	7.6%	0.0%	0.0%	53.5%	0.0%	0.0%	0.0%	0.0%	0.0%			
Dynamic, Static and Fluid (n = 54)	<i>n</i>	0	53	0	0	0	0	0	0	0	1	2073.85	<0.001	0.57
	%	0.0%	36.8%	0.0%	0.0%	0.0%	0.0%	0.0%	0.0%	0.0%	9.1%			
Dynamic and Absent (n = 11)	<i>n</i>	0	0	0	1	0	1	1	5	0	3	2073.85	<0.001	0.57
	%	0.0%	0.0%	0.0%	1.3%	0.0%	3.1%	5.6%	38.5%	0.0%	27.3%			
Static and Absent (n = 30)	<i>n</i>	0	0	5	1	2	17	0	3	1	1	2073.85	<0.001	0.57
	%	0.0%	0.0%	5.3%	1.3%	2.8%	53.1%	0.0%	23.1%	6.3%	9.1%			

Abbreviations: M- mass; N- nodule; n- number of animals; p - statistical significance; S- shred; T- tissue; W- wedge; Vc - effect size; χ^2 - chi square test result.

Analysis of Vascularity

The results of vascularity for airless subpleural tissue regions are presented in Table 5, with examples shown in Figures 2A-E. The analysis showed a statistically significant difference between the compared types of airless lung tissue with respect to vascularityization ($Vc > 0.50$). Tree-like

vascularization was most often observed in shred signs ($P<0.001$). In mass consolidations, the most common type of vascularity was chaotic and penetrating from the chest wall, along with a combination of the aforementioned types ($P<0.001$). Within nodule signs, chaotic vascularization was most often observed ($P<0.001$). Residual vascularization was more frequent within tissue signs ($P<0.001$). The vascular sign was observed significantly more often within wedge signs. In the complex lesion consisting of mass and tissue signs, chaotic vascularization and vascularization penetrating from the chest wall, or their combination was most often observed. In the complex lesion of a shred and wedge sign, the *vascular sign* was most frequently observed. In the complex lesion of mass and nodule sign, chaotic vascularization was observed most often while residual vascularization was observed most often in the complex shred and tissue sign lesions.

Table 5. Comparison of airless lung tissue types in terms of vascularity.

Vascularisation type	Consolidation type											χ^2	<i>p</i>	Vc
	S	S/T	M	N	T	M/T	W	S/W	M/N	S/N				
Tree (n = 173)	<i>n</i>	146	24	0	0	1	0	0	0	0	2	1011.32	<0.001	0.69
	%	88.0%	30.0%	0.0%	0.0%	2.7%	0.0%	0.0%	0.0%	0.0%	33.3%			
Residual (n = 119)	<i>n</i>	19	56	0	1	35	3	0	0	1	4			
	%	11.4%	70.0%	0.0%	14.3%	94.6%	13.0%	0.0%	0.0%	9.1%	66.7%			
Chaotic (n = 91)	<i>n</i>	0	0	59	6	0	16	0	0	10	0			
	%	0.0%	0.0%	86.8%	85.7%	0.0%	69.6%	0.0%	0.0%	90.9%	0.0%			
Chaotic and penetrating (n = 8)	<i>n</i>	0	0	6	0	0	2	0	0	0	0			
	%	0.0%	0.0%	8.8%	0.0%	0.0%	8.7%	0.0%	0.0%	0.0%	0.0%			
Penetrating (n = 5)	<i>n</i>	0	0	3	0	0	2	0	0	0	0			
	%	0.0%	0.0%	4.4%	0.0%	0.0%	8.7%	0.0%	0.0%	0.0%	0.0%			
Vascular sign (n = 31)	<i>n</i>	1	0	0	0	1	0	17	12	0	0			
	%	0.6%	0.0%	0.0%	0.0%	0.0%	2.7%	0.0%	100.0%	100.0%	0.0%			

Abbreviations: M-mass; n - number of observations; N- nodule; p - statistical significance; S- shred; T-tissue; W-wedge; Vc - effect size; Vs - vascular sign; χ^2 - chi square test result.

Analysis of Types of Consolidations in Terms of Diagnosis

There was a statistically significant difference between the types of consolidations and final presumed diagnosis (Table 6). Moreover, the obtained effect was strong ($Vc > 0.50$). There were 633 cases with only one classification of consolidation. The shred sign was observed most often in presumed cases of ARDS, parenchymal lung disease (PLD), pneumonia, pneumonia with PLD, and pneumonia with CHF. The mass type of consolidation was noted most often in tumors, tumors with concurrent atelectasis, and tumors with concurrent CHF. Nodule signs were seen significantly more often in cases that had metastases, granulomas, and tumors with concurrent granulomas [24]. Wedge signs were seen significantly more often in cases that had a final diagnosis of pulmonary thromboembolism (PTE), pneumonia with PTE, PTE with ARDS, and PTE with CHF. Finally, tissue signs were seen most often in cases with and CHF, atelectasis, and the cases with a combination of atelectasis and CHF.

Table 6. Comparison of airless lung tissue types in terms of diagnosis.

Diagnosis		Consolidation type											χ^2	<i>p</i>	Vc
		S	S/T	M	N	T	M/T	W	S/W	M/N	S/N				
ARDS (n = 32)	<i>n</i>	29	0	0	0	2	0	1	0	0	0	5040.92	<0.001	0.76	
	%	6.3%	0.0%	0.0%	0.0%	2.6%	0.0%	4.0%	0.0%	0.0%	0.0%				
PLD (n = 36)	<i>n</i>	33	2	0	0	0	0	1	0	0	0	5040.92	<0.001	0.76	
	%	7.2%	1.4%	0.0%	0.0%	0.0%	0.0%	4.0%	0.0%	0.0%	0.0%				
Tumor (n = 94)	<i>n</i>	1	0	80	5	2	4	0	0	1	1	5040.92	<0.001	0.76	
	%	0.2%	0.0%	81.6%	6.1%	2.6%	12.9%	0.0%	0.0%	5.6%	7.7%				
Tumor/Atelectasis (n = 42)	<i>n</i>	0	1	11	1	3	25	0	0	1	0	5040.92	<0.001	0.76	
	%	0.0%	0.7%	11.2%	1.2%	3.9%	80.6%	0.0%	0.0%	5.6%	0.0%				
Tumor/Metastasis (n = 24)	<i>n</i>	0	0	3	5	0	0	0	0	16	2	5040.92	<0.001	0.76	
	%	0.0%	0.0%	3.1%	6.1%	0.0%	0.0%	0.0%	0.0%	88.9%	15.4%				
Tumor/Granuloma (n = 1)	<i>n</i>	0	0	0	1	0	0	0	0	0	0	5040.92	<0.001	0.76	
	%	0.0%	0.0%	0.0%	1.2%	0.0%	0.0%	0.0%	0.0%	0.0%	0.0%				
Tumor/CHF (n = 3)	<i>n</i>	0	0	2	0	0	1	0	0	0	0	5040.92	<0.001	0.76	
	%	0.0%	0.0%	2.0%	0.0%	0.0%	3.2%	0.0%	0.0%	0.0%	0.0%				
Atelectasis (n = 41)	<i>n</i>	1	8	0	0	30	0	0	0	0	1	5040.92	<0.001	0.76	
	%	0.2%	5.5%	0.0%	0.0%	39.0%	0.0%	0.0%	0.0%	0.0%	7.7%				
Atelectasis/HF (n = 24)	<i>n</i>	0	1	0	0	23	0	0	0	0	0	5040.92	<0.001	0.76	
	%	0.0%	0.7%	0.0%	0.0%	29.9%	0.0%	0.0%	0.0%	0.0%	0.0%				
Atelectasis/CHF/Parenchymal lung disease (n = 1)	<i>n</i>	0	1	0	0	0	0	0	0	0	0	5040.92	<0.001	0.76	
	%	0.0%	0.7%	0.0%	0.0%	0.0%	0.0%	0.0%	0.0%	0.0%	0.0%				
Pulmonary edema (n = 1)	<i>n</i>	1	0	0	0	0	0	0	0	0	0	5040.92	<0.001	0.76	
	%	0.2%	0.0%	0.0%	0.0%	0.0%	0.0%	0.0%	0.0%	0.0%	0.0%				
Metastases (n = 65)	<i>n</i>	0	0	0	64	0	0	0	0	0	1	5040.92	<0.001	0.76	
	%	0.0%	0.0%	0.0%	78.0%	0.0%	0.0%	0.0%	0.0%	0.0%	7.7%				
Metastases/Atelectasis (n = 5)	<i>n</i>	0	0	0	2	0	0	0	0	0	3	5040.92	<0.001	0.76	
	%	0.0%	0.0%	0.0%	2.4%	0.0%	0.0%	0.0%	0.0%	0.0%	23.1%				
Pneumonia/ARDS (n = 15)	<i>n</i>	10	3	0	0	0	0	1	1	0	0	5040.92	<0.001	0.76	
	%	2.2%	2.1%	0.0%	0.0%	0.0%	0.0%	4.0%	5.3%	0.0%	0.0%				
Pneumonia (n = 281)	<i>n</i>	248	30	0	0	2	0	0	0	0	1	5040.92	<0.001	0.76	
	%	53.9%	20.7%	0.0%	0.0%	2.6%	0.0%	0.0%	0.0%	0.0%	7.7%				
Pneumonia/PLD (n = 23)	<i>n</i>	19	4	0	0	0	0	0	0	0	0	5040.92	<0.001	0.76	
	%	4.1%	2.8%	0.0%	0.0%	0.0%	0.0%	0.0%	0.0%	0.0%	0.0%				
Pneumonia/Atelectasis (n = 111)	<i>n</i>	17	84	1	0	6	1	0	0	0	2	5040.92	<0.001	0.76	
	%	3.7%	57.9%	1.0%	0.0%	7.8%	3.2%	0.0%	0.0%	0.0%	15.4%				
Pneumonia/Atelectasis/CHF (n = 2)	<i>n</i>	0	8	0	0	2	0	0	0	0	0	5040.92	<0.001	0.76	
	%	0.0%	5.5%	0.0%	0.0%	2.6%	0.0%	0.0%	0.0%	0.0%	0.0%				

Pneumonia/Abscess (n = 3)	<i>n</i>	0	0	1	0	1	0	0	0	0	1	
	%	0.0%	0.0%	1.0%	0.0%	1.3%	0.0%	0.0%	0.0%	0.0%	7.7%	
Pneumonia/PTE (n = 15)	<i>n</i>	0	0	0	0	0	0	3	12	0	0	
	%	0.0%	0.0%	0.0%	0.0%	0.0%	0.0%	12.0%	63.2%	0.0%	0.0%	
Pneumonia/ PTE /ARDS (n = 2)	<i>n</i>	0	0	0	0	0	0	0	2	0	0	
	%	0.0%	0.0%	0.0%	0.0%	0.0%	0.0%	0.0%	10.5%	0.0%	0.0%	
Pneumonia/Granuloma (n = 1)	<i>n</i>	0	0	0	0	0	0	0	0	0	1	
	%	0.0%	0.0%	0.0%	0.0%	0.0%	0.0%	0.0%	0.0%	0.0%	7.7%	
Pneumonia/CHF (n = 103)	<i>n</i>	98	3	0	0	2	0	0	0	0	0	
	%	21.3%	2.1%	0.0%	0.0%	2.6%	0.0%	0.0%	0.0%	0.0%	0.0%	
Pneumonia/ CHF/tracheal collapse (n = 1)	<i>n</i>	1	0	0	0	0	0	0	0	0	0	
	%	0.2%	0.0%	0.0%	0.0%	0.0%	0.0%	0.0%	0.0%	0.0%	0.0%	
PTE (n = 18)	<i>n</i>	1	0	0	0	0	0	14	3	0	0	
	%	0.2%	0.0%	0.0%	0.0%	0.0%	0.0%	56.0%	15.8%	0.0%	0.0%	
Metastases/ARDS (n = 5)	<i>n</i>	0	0	0	0	1	0	4	0	0	0	
	%	0.0%	0.0%	0.0%	0.0%	1.3%	0.0%	16.0%	0.0%	0.0%	0.0%	
PTE/Metastasis (n = 0)	<i>n</i>	0	0	0	0	0	0	0	0	0	0	
	%	0.0%	0.0%	0.0%	0.0%	0.0%	0.0%	0.0%	0.0%	0.0%	0.0%	
PTE/CHF (n = 2)	<i>n</i>	0	0	0	0	0	0	1	1	0	0	
	%	0.0%	0.0%	0.0%	0.0%	0.0%	0.0%	4.0%	5.3%	0.0%	0.0%	
Granuloma (n = 4)	<i>n</i>	0	0	0	4	0	0	0	0	0	0	
	%	0.0%	0.0%	0.0%	4.9%	0.0%	0.0%	0.0%	0.0%	0.0%	0.0%	
CHF (n = 4)	<i>n</i>	1	0	0	0	3	0	0	0	0	0	
	%	0.2%	0.0%	0.0%	0.0%	3.9%	0.0%	0.0%	0.0%	0.0%	0.0%	

Abbreviations: CHF- congestive heart failure; M-mass; N-nodule; p - statistical significance; PLD – parenchymal lung disease; PTE – pulmonary thromboembolic disease; S-shred; T-tissue; W-wedge; Vc - effect size; χ^2 – chi-square test result.

In 348 cases, complex consolidations or two different airless tissue patterns were present. The finding of shred and tissue signs were often seen in cases diagnosed with combined atelectasis, CHF and PLD, cases with pneumonia and atelectasis, and cases with pneumonia, atelectasis and CHF. Complex cases with findings of mass plus tissue consolidation were seen in cases most often diagnosed with as having tumors with atelectasis, and tumors with CHF. Shred and wedge signs were often seen together in cases with a presumed diagnosis of PTE, pneumonia with PTE, pneumonia with PTE and ARDS, and PTE with CHF. Mass combined with nodule signs were seen in cases suspected to have tumors with metastases. Complex cases with findings of shred sign and mass signs were seen most frequently in presumed cases with tumors and metastases, and pneumonia with abscesses.

Discussion

This study demonstrates that it is possible to describe the vascular patterns of subpleural lung tissue in cats and dogs. Furthermore, classification of vascular patterns in sonographically identifiable shred, tissue, nodule, and wedge signs, and mass lesions, appears to differ between different lung

pathologies. This is important, as it may influence further help narrow differential diagnosis and direct further diagnostic findings. For example, in human medicine, the identification of even a single peripheral wedge sign with a vascular sign is an indicator for further diagnostic tests to confirm PTE [8]. Therefore, if present, the identification of airless lung tissue and its classification, including vascular and bronchogram patterns should prompt consideration of further diagnostic testing in cats and dogs. However, it is important to always be interpret LUS finding considering all additional clinical and diagnostic findings [8,31].

Airless subpleural lung tissue may develop due to various etiologies and their vascular morphological and hemodynamic changes have been investigated in human medicine. Pulmonary vascularization in animals and humans has organ-specific characteristics due to the dual arterial supply of the lungs [25,32]. Pulmonary arteries show a treelike pattern. Their branches course centrifugally and react to hypoxia by vasoconstriction induced by the Euler-Liljestrand reflex [25], which can explain residual blood flow in atelectasis [32,33]. The vascularity of a consolidated lung area is not possible to assess on TXR, and CT is still an expensive and often less accessible method compared to standard ultrasonography, leaving the latter as a feasible diagnostic modality. From the clinical point of view, information about vascularity, type of bronchogram, or its absence in airless subpleural lung tissue may have clinical significance and may influence further diagnostic decisions.

In the human literature there are 4 typical vascular patterns described within tissue-like lesions, which were all present in cats and dogs of the current study [25,34,35]. Anatomical tree-like vascularization is seen in humans with pneumonia, which was also the case in our study, where cats and dogs with presumed pneumonia also had anatomical tree-like patterns. The shape of those consolidations was irregular. Color Doppler blood flow tended to appear and disappear with the heartbeat in these cases. The second type of vascularity, termed residual vascularization, was found in cases of atelectasis (i.e. the tissue sign) in the current study, which is similarly reported in humans. Vascularization may be reduced by a mass compressing the vessels centrally within the region of atelectasis, vasoconstriction in cases of chronic pneumonia, or secondary to significant pleural effusion in cases with severe congestive heart failure. In tumors, residual vascularization or chaotic vascularization was present, but there was no air or fluid bronchograms noted in these cases. Neoplastic lesions often obtain nutrients from oxygen-rich blood [32,33]. The anatomical structure of tumors was destroyed in some cases, likely as a result of calcifications which appeared as small hyperechoic round dots. The third vascularization type was identified within masses, which demonstrated vessels that traverse the thoracic wall to enter the region of lung consolidation. It is believed that neovascularization of lung masses in these cases arise from the intercostal arteries, which are rich in oxygen [36]. The last observed pattern was the "vascular sign." The "vascular sign" is believed to result from vessel occlusion by embolic material. Abrupt cessation of blood flow at the "tip" of the consolidation can be seen on color Doppler. The consolidation is usually triangular or basket-shaped and hypoechoic; in the literature, it's called a "wedge sign." The "vascular sign" was present in dogs infested with *Angiostrongylus vasorum* [3] and cats with various types of cardiomyopathy, causing spontaneous echocontrast in the right atrium. In 1 case, thromboembolic lung disease was confirmed on postmortem examination. The "vascular sign" was also seen in 7 dogs that presented with severe dyspnea that did not have a final diagnosis, all of which were Yorkshire Terriers, which were all being treated for Cushing's disease. These dogs were euthanized due to lack of response to treatment.

Interestingly, in this retrospective analysis, various complex lesions were described, which indicates the commonality of simultaneous comorbidities — for example, finding CHF with shred signs suggests coexisting pulmonary edema and pneumonia. Humans with CHF classically have an absence of pleural line and subplueral abnormalities [8,37]. However, we observed changes in the pleural line, most commonly in gravity-dependent lung regions, in cases with severe pulmonary edema. Despite this, the shred sign was observed in cases of CHF with coexisting pneumonia. The complex lesions consisting of mass and atelectasis were better visualized on the LUS than TRX. The identification of bronchograms and vascular patterns increased the suspicion of a neoplastic process

within one case diagnosed with atelectatic lung. In this case resorption atelectasis was identified peripheral to the neoplastic lesion.

This study has several limitations. A general drawback of color Doppler sonography for LUS is that motion artifacts secondary to respirations may interfere with the quality of color Doppler sonography. Good ultrasound settings and Doppler velocity scale adjustments are essential to visualize small vessels within lung consolidations. Doppler analysis can be challenging to perform for less experienced operators. Nevertheless, regions of airless subpleural lung tissue should be evaluated with respect to their bronchograms and vascularity whenever possible. If the patient is in severe respiratory distress or panting, LUS can be performed following patients' stabilization and/or sedation/anxiolytics are administered. LUS should be performed as soon as possible following sedation to avoid possible atelectasis, which may occur secondary to prolonged lateral recumbency.

Another limitation of this study is that lesions that fail to reach the lung periphery will not be detected. This is because lung pathology located below the lung surface will be obscured by overlying air, with only reverberation artifacts being seen [38]. Therefore, LUS cannot rule out lung pathology that is located within deeper lung tissues. Despite this, a lot of lung pathology, such as metastases, will occur close to the lung surface, and will therefore be seen on LUS [39,40].

Conclusions

This study demonstrates that the analysis of the shape, and characterization of bronchogram, and vascularity of airless subpleural lung tissue is possible in cats and dogs and that findings varied between patients with different lung pathologies. This may prove helpful in differentiating underlying etiologies and directing further diagnostics, although further prospective clinical research would be required to confirm the sensitivity and specificity of these findings with relation to different disease processes. Characterization of subpleural lung tissue in cats and dogs may also suggest respiratory pathology is multifactorial in origin when identified on LUS.

Supplementary Materials: The following supporting information can be downloaded at the website of this paper posted on Preprints.org. Movie 1. Linear probe, lung preset. Color Doppler imaging of an anatomical tree-like vascular pattern in a dog with pneumonia. Movie 2. Linear probe, lung preset. Color Doppler imaging of a residual vascular pattern within a region of lung consolidation. Movie 3. Linear probe, thyroid preset. Color Doppler imaging of a penetrating vascular penetrating extending from the chest wall. Movie 4. Linear probe, Lung preset. Color Doppler imaging showing abrupt cessation of blood flow at the "tip" of a region of consolidation "*vascular sign*" (→), C-line (←) hypoechoic triangular shape consolidation (↓).

Abbreviations

ARDS	acute respiratory distress syndrome
BAL	bronchoalveolar lavage
CD	color doppler
CHF	congestive heart failure
CT	computed tomography
FNA	fine needle aspiration
LUS	lung ultrasound
M	mass
N	nodule type consolidation
PD	power doppler
PLD	parenchymal lung disease
PTE	pulmonary thromboembolism
TRX	thoracic radiograph
S	shred type consolidation

T	tissue type consolidation
W	wedge type consolidation

References

1. Pelchat J, Chalhoub S, Boysen SR. The use of veterinary point-of-care ultrasound by veterinarians: A nationwide Canadian survey. *Can Vet J* 2020;61:1278-1282.
2. Ward JL, DeFrancesco TC. The Role of Point-of-Care Ultrasound in Managing Cardiac Emergencies. *Vet Clin North Am Small Anim Pract* 2023.
3. Kraszewska K GM, Boysen S. Case report: Application of color Doppler sonography for the assessment of pulmonary consolidations in a dog. *Frontiers in Veterinary Science* 2023;10.
4. Fernandes Rodrigues N, Giraud L, Bolen G, et al. Comparison of lung ultrasound, chest radiographs, C-reactive protein, and clinical findings in dogs treated for aspiration pneumonia. *J Vet Intern Med* 2022;36:743-752.
5. Venco L, Colaneri G, Formaggini L, et al. Utility of thoracic ultrasonography in a rapid diagnosis of angiostrongylosis in young dogs presenting with respiratory distress. *Vet J* 2021;271:105649.
6. Łobaczewski A, Czopowicz M, Moroz A, et al. Integrated Basic Heart and Lung Ultrasound Examination for the Differentiation between Bacterial Pneumonia and Lung Neoplasm in Dogs-A New Diagnostic Algorithm. *Animals (Basel)* 2022;12.
7. Lin CH, Lo PY, Lam MC, et al. Usefulness of Chest Ultrasonography in Predicting Diagnosis in Non-emergency Small Animal Patients With Lung Parenchymal and Pleural Disease. *Front Vet Sci* 2020;7:616882.
8. Buda N, Kosiak W, Radzikowska E, et al. Polish recommendations for lung ultrasound in internal medicine (POLLUS-IM). *J Ultrason* 2018;18:198-206.
9. Volpicelli G, Silva F, Radeos M. Real-time lung ultrasound for the diagnosis of alveolar consolidation and interstitial syndrome in the emergency department. *Eur J Emerg Med* 2010;17:63-72.
10. Demi L, Wolfram F, Klersy C, et al. New International Guidelines and Consensus on the Use of Lung Ultrasound. *J Ultrasound Med* 2023;42:309-344.
11. Copetti R, Soldati G, Copetti P. Chest sonography: a useful tool to differentiate acute cardiogenic pulmonary edema from acute respiratory distress syndrome. *Cardiovasc Ultrasound* 2008;6:16.
12. Huang D, Ma H, Xiao Z, et al. Diagnostic value of cardiopulmonary ultrasound in elderly patients with acute respiratory distress syndrome. *BMC Pulm Med* 2018;18:136.
13. Lichtenstein DA, Meziere GA. Relevance of lung ultrasound in the diagnosis of acute respiratory failure: the BLUE protocol. *Chest* 2008;134:117-125.
14. Kameda T, Kamiyama N, Taniguchi N. The Mechanisms Underlying Vertical Artifacts in Lung Ultrasound and Their Proper Utilization for the Evaluation of Cardiogenic Pulmonary Edema. *Diagnostics (Basel)* 2022;12.
15. Schmickl CN, Menon AA, Dhokarh R, et al. Optimizing B-lines on lung ultrasound: an in-vitro to in-vivo pilot study with clinical implications. *J Clin Monit Comput* 2020;34:277-284.
16. Matthias I, Panebianco NL, Maltenfort MG, et al. Effect of Machine Settings on Ultrasound Assessment of B-lines. *J Ultrasound Med* 2020;40:2039-2046.
17. Yuan A, Yang PC, Lee L, et al. Reactive pulmonary artery vasoconstriction in pulmonary consolidation evaluated by color Doppler ultrasonography. *Ultrasound Med Biol* 2000;26:49-56.
18. Luis Fuentes V, Abbott J, Chetboul V, et al. ACVIM consensus statement guidelines for the classification, diagnosis, and management of cardiomyopathies in cats. *J Vet Intern Med* 2020;34:1062-1077.
19. Reinero C, Visser LC, Kelliher HB, et al. ACVIM consensus statement guidelines for the diagnosis, classification, treatment, and monitoring of pulmonary hypertension in dogs. *J Vet Intern Med* 2020;34:549-573.
20. Lichtenstein DA. Lung Ultrasound in the Critically Ill. London Springer 2016;376.
21. Lisciandro GR, Lisciandro SC. Lung Ultrasound Fundamentals, "Wet Versus Dry" Lung, Signs of Consolidation in Dogs and Cats. *Vet Clin North Am Small Anim Pract* 2021;51:1125-1140.

22. Lisciandro GR, Puchot ML, Gambino JM, et al. The wedge sign: A possible lung ultrasound sign for pulmonary thromboembolism. *J Vet Emerg Crit Care* (San Antonio) 2022.
23. Boysen RSC, S. Gommeren, K. The Essentials of Veterinary Point of Care Ultrasound: Pleural Space and LungEdra Publishing 2022.
24. Yang PC, Luh KT, Wu HD, et al. Lung tumors associated with obstructive pneumonitis: US studies. *Radiology* 1990;174:717-720.
25. Gorg C, Seifart U, Gorg K, et al. Color Doppler sonographic mapping of pulmonary lesions: evidence of dual arterial supply by spectral analysis. *J Ultrasound Med* 2003;22:1033-1039.
26. Yuan A, Yang PC, Chang DB. Pulmonary infarction: use of color Doppler sonography for diagnosis and assessment of reperfusion of the lung. *AJR Am J Roentgenol* 1993;160:419-420.
27. Buda N, Kosiak W. Is a linear probe helpful in diagnosing diseases of pulmonary interstitial spaces? *J Ultrason* 2017;17:136-141.
28. Sripathi S, Mahajan A. Comparative study evaluating the role of color Doppler sonography and computed tomography in predicting chest wall invasion by lung tumors. *J Ultrasound Med* 2013;32:1539-1546.
29. Yuan A, Chang DB, Yu CJ, et al. Color Doppler sonography of benign and malignant pulmonary masses. *AJR Am J Roentgenol* 1994;163:545-549.
30. Gorg C, Bert T. Transcutaneous colour Doppler sonography of lung consolidations: review and pictorial essay. Part 1: pathophysiologic and colour Doppler sonographic basics of pulmonary vascularity. *Ultraschall Med* 2004;25:221-226.
31. Buda N, Kosiak W, Wehnicki M, et al. Recommendations for Lung Ultrasound in Internal Medicine. *Diagnostics* (Basel) 2020;10.
32. Rick T, Kleiter M, Schwendenwein I, et al. Contrast-enhanced ultrasonography characteristics of intrathoracic mass lesions in 36 dogs and 24 cats. *Vet Radiol Ultrasound* 2019;60:56-64.
33. Linta N, Baron Toaldo M, Bettini G, et al. The feasibility of contrast enhanced ultrasonography (CEUS) in the diagnosis of non-cardiac thoracic disorders of dogs and cats. *BMC Vet Res* 2017;13:141.
34. Yang PC. Color doppler ultrasound of pulmonary consolidation. *European Journal of Ultrasound* 1996;3:169-178.
35. Hsu WH, Ikezoe J, Chen CY, et al. Color Doppler ultrasound signals of thoracic lesions. Correlation with resected histologic specimens. *Am J Respir Crit Care Med* 1996;153:1938-1951.
36. Mathis G, Gehmacher O. Ultrasound-guided diagnostic and therapeutic interventions in peripheral pulmonary masses. *Wien Klin Wochenschr* 1999;111:230-235.
37. Buda N, Kosiak W, Wehnicki M, et al. Recommendations for Lung Ultrasound in Internal Medicine. *Diagnostics* (Basel) 2020;10.
38. Mathis G. Thoraxsonography--Part II: Peripheral pulmonary consolidation. *Ultrasound Med Biol* 1997;23:1141-1153.
39. Pacholec C, Lisciandro GR, Masseau I, et al. Lung ultrasound nodule sign for detection of pulmonary nodule lesions in dogs: Comparison to thoracic radiography using computed tomography as the criterion standard. *Vet J* 2021;275:105727.
40. Johnson VS, Ramsey IK, Thompson H, et al. Thoracic high-resolution computed tomography in the diagnosis of metastatic carcinoma. *J Small Anim Pract* 2004;45:134-143.

Disclaimer/Publisher's Note: The statements, opinions and data contained in all publications are solely those of the individual author(s) and contributor(s) and not of MDPI and/or the editor(s). MDPI and/or the editor(s) disclaim responsibility for any injury to people or property resulting from any ideas, methods, instructions or products referred to in the content.